Glacial isostatic adjustment associated with the Barents Sea ice sheet: a modelling inter-comparison

A. Auriac[1,*], P. L. Whitehouse[1], M. J. Bentley[1], H. Patton[2], J. M. Lloyd[1] and A. Hubbard[2]

[1] *Department of Geography, Durham University, South Road, Durham, DH1 3LE, UK*

[2] *CAGE - Centre for Arctic Gas Hydrate, Environment and Climate, Department of Geology, University of Tromsø, N-9037 Tromsø, Norway*

[*] *a.m.auriac@durham.ac.uk, +44 191 334 1943*

Keywords: glacial isostatic adjustment modelling; ice sheet; Barents Sea; relative sea level

Abstract

The 3D geometrical evolution of the Barents Sea Ice Sheet (BSIS), particularly during its late-glacial retreat phase, remains largely ambiguous due to the paucity of direct marine- and terrestrial-based evidence constraining its horizontal and vertical extent and chronology. One way of validating the

numerous BSIS reconstructions previously proposed is to collate and apply them under a wide range of Earth models and to compare prognostic (isostatic) output through time with known relative sea-level (RSL) data. Here we compare six contrasting BSIS load scenarios via a spherical Earth system model and derive a best-fit, χ^2 parameter using RSL data from the four main terrestrial regions within the domain: Svalbard, Franz Josef Land, Novaya Zemlya and northern Norway. Poor χ^2 values allow two load scenarios to be dismissed, leaving four that agree well with RSL observations. The remaining four scenarios optimally fit the RSL data when combined with Earth models that have an upper mantle viscosity of 0.2–2$\times10^{21}$ Pa s, while there is less sensitivity to the lithosphere thickness (ranging from 71 to 120 km) and lower mantle viscosity (spanning 1–50$\times10^{21}$ Pa s). GPS observations are also compared with predictions of present-day uplift across the Barents Sea. Key locations where relative sea-level and GPS data would prove critical in constraining future ice-sheet modelling efforts are also identified.

1 Introduction

The Barents Sea, bordered by Norway and Russia to the south, Svalbard to the north and Novaya Zemlya to the east (Fig. 1), was extensively covered by an ice sheet during the last glacial cycle and experienced at least three shelf-wide glaciations during that period (Mangerud et al., 1998). Significant debate existed in the past over the extent (restricted to extensive) of the ice cover during the last glacial maximum, or LGM (e.g. Boulton, 1979;

Hughes et al., 1977; Grosswald and Hughes, 2002), which occurred in this northerly region slightly later than the global LGM (Clark et al., 2009). It is, however, now more widely accepted that a single extensive grounded ice sheet was present over the Barents Sea during the last glaciation (Svendsen et al., 2004; Patton et al., 2015; Hughes et al., 2016), which fully or partially covered Svalbard, Franz Josef Land and Novaya Zemlya, and coalesced with the Fennoscandian ice sheet in the south. This consensus has been reached following the collection and analysis of a large amount of terrestrial and marine-based geophysical data in recent years (e.g. Mangerud et al., 1999; Ottesen et al., 2005; Andreassen et al., 2008; Hormes et al., 2013). In the western part of the Barents Sea, the extent of the ice sheet and pattern of deglaciation after the LGM is relatively well known (e.g. Landvik et al., 1998; Winsborrow et al., 2010; Ingólfsson and Landvik, 2013). Significant uncertainties, however, still remain regarding its precise extent, its thickness evolution and the timing of deglaciation in the central and eastern sector of the Barents Sea which has received less attention (Polyak et al., 1997, 2008; Bjarnadóttir et al., 2014; Patton et al., 2015; Hughes et al., 2016).

One means to improve the state-of-knowledge regarding the 3D ice extent and deglacial timing is through modelling of the glacial isostatic adjustment (GIA) signal resulting from the ice loading and unloading. We aim here to use a GIA model to test different ice load scenarios so as to better understand former ice extent in the Barents Sea over the last glacial cycle. We achieve this by solving the sea-level equation in the manner of Mitrovica and Milne (2003), using six different ice load scenarios that are available for this

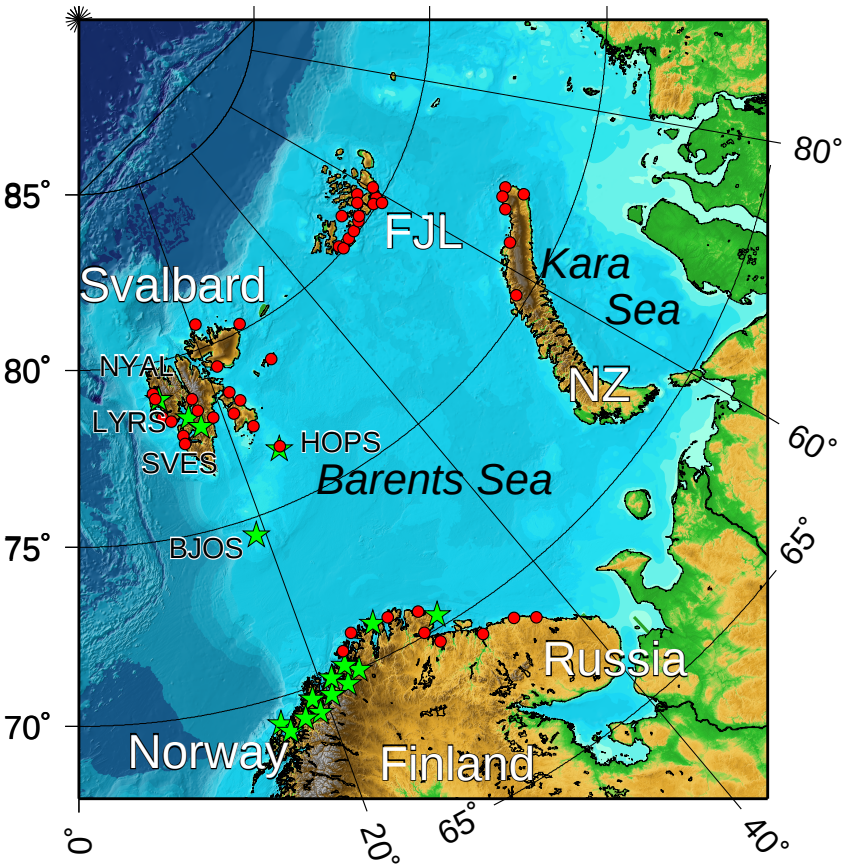

Figure 1: Bathymetry of the Barents Sea and surrounding land masses (FJL: Franz Josef Land, NZ: Novaya Zemlya). GPS stations (and their names in Svalbard) as well as locations of relative sea-level (RSL) data used in this study are indicated with green stars and red circles, respectively.

region (five published and one currently being developed). We use published relative sea-level (RSL) data bordering the Barents Sea, assembled in a consistent manner into one database, to investigate the accuracy of the different ice load scenarios available for this area and to infer which one provides an overall best fit to the local sea-level history. By comparing the RSL data with the model predictions, we also solve for the optimal Earth rheology in this region. Finally, we compare the present-day uplift prediction, obtained from our best-fit model, with GPS data from Svalbard and Scandinavia, and identify key locations that can be used in the future to better constrain the ice sheet reconstruction.

2 GIA modelling

2.1 Numerical code

We solve the sea-level equation (first derived by Farrell and Clark, 1976) using the implementation from Mitrovica and Milne (2003) and Kendall et al. (2005). Gravitationally self-consistent sea-level changes are computed, taking into account shoreline evolution as well as the time-dependent evolution of marine-based ice margins. The sea-level equation is solved iteratively using an extended pseudo-spectral algorithm.

This numerical code assumes a spherically symmetric Earth, whose properties are based on the Preliminary Reference Earth Model, or PREM (Dziewon-

ski and Anderson, 1981). The Earth model is implemented as an input with three variables: lithosphere thickness and upper and lower mantle viscosity. We use 300 different Earth models, where the lithosphere thickness ranges from 46 to 120 km and the upper and lower mantle viscosities range from 0.05×10^{21} to 5×10^{21} Pa s and 1×10^{21} to 50×10^{21} Pa s, respectively. These Earth models cover the range of Earth parameters generally found or inferred for this area from a range of geophysical techniques (e.g. Steffen and Kaufmann, 2005; Kaufmann and Wolf, 1996; Klitzke et al., 2014). The second input required for the GIA model is the history of ice loading (see Section 2.2), giving the distribution of ice (extent and thickness) at the surface of the Earth at specific times during the last glacial cycle (i.e. 122 ka BP to present).

After solving the sea-level equation, we derive an estimate of the present-day rate of surface deformation across the Barents Sea, and we determine the time evolution of the sea level at specific locations. These are the two main outputs we will utilize in this study for comparison against field data.

2.2 Ice loading scenarios

Six different ice loading scenarios over the Barents Sea area are tested based on: (i) the ICE-5G scenario (Peltier, 2004), (ii) the ICE-6G_C scenario (Argus et al., 2014; Peltier et al., 2015), (iii) the ANU scenario (Lambeck et al., 2010), (iv) the model developed by Näslund et al. (2005); Näslund (2006), henceforth referred to as the N05 scenario, (v) the model developed by Siegert

Table 1: General characteristics of the ice load scenarios used in this study.

Scenario name	Reference	Spatial coverage[1]	Temporal coverage [ka BP]
ICE-5G	Peltier (2004)	global	122 – 0
ICE-6G_C	Argus et al. (2014); Peltier et al. (2015)	global	26 – 0
ANU	Lambeck et al. (2010)	global	122 – 0
N05	Näslund et al. (2005); Näslund (2006)	local	122 – 0
S04	Siegert and Dowdeswell (2004)	local	32 – 12
UiT	this study	local	35 – 7.5

[1] "Local" implies that ice thickness estimates are given for the Fennoscandian and Barents Sea ice sheets only.

and Dowdeswell (2004), henceforth referred to as the S04 scenario, and (vi) the University of Tromsø, UiT, scenario. The main characteristics of each model are presented in Table 1, including the name given to each model, as used in the rest of the study, and the spatial and temporal coverage of each scenario. Three of the models are only defined locally for Scandinavia and the Barents Sea, while the others (ICE-5G, ICE-6G_C and ANU) define global ice sheet changes. The ICE-5G scenario has a lower spatial resolution (1 degree grid) than the other models, however, for modelling purposes, all the scenarios are resampled to a spherical harmonic truncation level of degree and order 256.

Each of the ice loading scenarios has been produced using different methods and sets of constraints and it is important to consider the relative merits and limitations of each. In essence though, the six scenarios can be divided into two main types of approach: i) those based on isostatic adjustment mod-

elling (ICE-5G, ICE-6G_C and ANU) that use RSL data and dated margins to inversely constrain an optimal ice loading pattern, and, ii) those based on forward, time-dependent ice flow modelling (NO5, SO4 and UiT) that are forced by past climate change and mass-balance distribution to yield the free evolution of horizontal ice thickness through time.

The ICE-5G scenario (Peltier, 2004) is constrained by dated observations of ice sheet margins, RSL curves and the global mean sea-level curve. It uses the radial viscosity model VM2 from Peltier (2004). We use the ICE-5G scenario with a wider range of Earth models in our modelling to test the effects of the Earth model chosen and study how well each of our free parameters is resolved by our method and data. Using a different Earth model to VM2 in the far field will not significantly alter the local deformation caused by the far-field loading. Moreover, although ICE-5G is constrained by RSL data, it has not been tested against many of the recently-published data that we include in this study. Thus, although a good fit to RSL data might be anticipated, one should not expect the fit between model predictions and observations to be perfect by default.

ICE-5G has been recently revised and updated to the ICE-6G_C scenario by Argus et al. (2014) and Peltier et al. (2015). It is built mostly on the same principles as its predecessor, but is constrained by an updated data set of geological observations (including relative sea-level data). Compared with its predecessor, the ICE-6G_C reconstruction uses the widest range of GPS observations available to constrain the model. A major improvement from

ICE-5G to ICE-6G_C comes from the new definition used for the Stokes gravity coefficients, as described by Chambers et al. (2010). The ICE-6G_C scenario has a higher temporal resolution over the last 26 ka compared with the ICE-5G scenario; and it has been developed in conjunction with the radial viscosity model VM5a. Once again, we tested this scenario against a wide range of Earth models, including an average of VM5a.

The ice extent and thickness of the ANU scenario (Lambeck, 1995; Lambeck et al., 1998, 2006, 2010, 2014) are obtained by analysing the response to surface loading on a linear, viscoelastic Maxwell, radially symmetric and compressible Earth. This model uses conservation of mass of the ocean-ice load and an equipotential ocean surface at all times. It takes into account rotational effects, the evolution of the ocean basins through time and grounding line migrations, and it includes water loading of ice-marginal lakes. The model is tuned using various geological and geophysical measurements such as relative sea-level data, tide gauge records, lake tilt measurements, GPS observations and paleo ice margin positions. The model inverts iteratively for the Earth rheology and ice load geometry. The range of effective lithosphere thickness, upper and lower mantle viscosity given by Lambeck et al. (2010) is inferred for Fennoscandia and may not necessarily be the optimum Earth rheology for the Barents Sea region. As with the ICE-5G and ICE-6G_C scenarios, we note that it is partly tuned to RSL data and this has implications for the fit to RSL observations is this paper.

The remaining three local ice load scenarios are all derived using time-

dependent coupled climate/thermomechanical ice flow models but, contrary to the global isostatic adjustment scenarios, they are not pre-tuned or conditioned to RSL data. They hence represent truly independent derivations of ice thickness distribution based on past-climate change alone and this is an important consideration when assessing their performance against available RSL results presented here. The N05 scenario was developed using the University of Maine Ice Sheet Model (UMISM) (Näslund et al., 2005; Näslund, 2006). It is a time-dependent, thermomechanical ice-sheet model in parts constrained by the geothermal heat flux at the bed, it uses the finite element method to solve the mass-, momentum- and energy-continuity equations, and the isostatic response of the Earth is modelled using a hydrostatically supported elastic plate. However, the geothermal heat flux is not well known for the Barents Sea. A moderate change in the geothermal heat flux would have measurable effects on the basal ice melt and would likely modify the predictions of ice thickness given by the modelling. Inputs to the ice-sheet model, which starts from a situation with no ice during the last interglacial, include air temperature (from Greenland ice cores, covering the past 120 ka) and precipitation as well as a digital elevation model of present-day topography. The model accounts for eustatic sea-level changes over the last 120 ka, using an independent sea-level curve to constrain the sea level contribution from far- field ice sheets. The N05 scenario is constrained using dated ice-marginal positions during Weichselian stadials.

The S04 scenario is built using an ice sheet model (based on the continuity equation for ice flow) coupled with a model of water-saturated basal

sediment deformation and transportation (Siegert et al., 1999; Siegert and Dowdeswell, 2004). Inputs to the ice-sheet model correspond to an initial bedrock topography at 30 ka BP (assumed similar to the present-day topography), which is automatically adjusted for ice loading of the crust using the isostasy method from Oerlemans and van der Veen (1984), a eustatic sea-level curve for the past 30 ka, a depth-related calving function, air temperature and precipitation changes. Model predictions are tuned to fit geological data (e.g. marginal sediments) via an inverse-type procedure, using eustatic sea level, air temperature and rate of calving as tuning parameters.

The UiT scenario is built using a first-order, thermomechanical, finite-difference model based on that used to previously reconstruct the British and Icelandic Last Glacial Maximum ice sheets (Hubbard et al., 2006; Hubbard, 2006; Hubbard et al., 2009). The model implements grounded ice-sheet and ice shelf equations developed and applied by Pollard and DeConto (2007), Marshall et al. (2005) and Hubbard (1999, 2000), which are iteratively solved to yield terms for the vertically-averaged longitudinal stress and basal traction. Surface mass balance is derived using a distributed degree-day calculation based on a reference seasonal climatology from mean (1950–2000) precipitation and temperature patterns (WorldClim, www.worldclim.org). The model is perturbed from this reference state by a scaled NGRIP oxygen isotope curve (NGRIP members, 2004, www.ncdc.noaa.gov/paleo/icecore/greenland/ngrip/ngrip-data.html), and a eustatic sea-level reconstruction derived from benthic isotopic records (Waelbroeck et al., 2002). An empirical depth-related calving algorithm is applied to the marine margin (Brown et al., 1982), and the iso-

static response to ice loading is computed using an elastic lithosphere/relaxed asthenosphere scheme (Le Meur and Huybrechts, 1996). Geothermal forcing is assumed constant at the continental background rate of 55 mWm^{-2}.

As for the global ice load scenarios, the three local reconstructions are tested on a range of Earth parameters to study the effect of the Earth model chosen and see how well the free parameters are resolved by our method. Moreover, the Earth model used to develop each of the local scenarios is not as realistic as the model implemented in our GIA model (Le Meur and Huybrechts, 1996), so they were not reproduced here.

Figs. 2 and 3 show the ice extent and thickness for each of the scenarios at two different periods: maximum extent at the LGM (occurring at different times depending on the scenario) and at a latter stage of deglaciation at 12.5 ka BP. There are large discrepancies between the models, not only at the times shown but for the whole time span of the reconstructions; these discrepencies are most apparent in the central Barents Sea. In general, the ICE-5G, ICE-6G_C and UiT scenarios predict a much thicker ice cover over the Barents Sea ($\sim$3000 m or greater) compared with the other models. The ICE-5G scenario also predicts an early ice dome centred in the north Barents Sea. The N05 scenario has the smallest ice extent at the LGM, with the Barents Sea and the Fennoscandian ice sheets linked only by a narrow strip of ice over the central Barents Sea (Fig. 3a), whereas all the other scenarios predict a single ice sheet covering the whole of the Barents Sea and Novaya Zemlya region at that time. The LGM in the Barents Sea also occurs at dif-

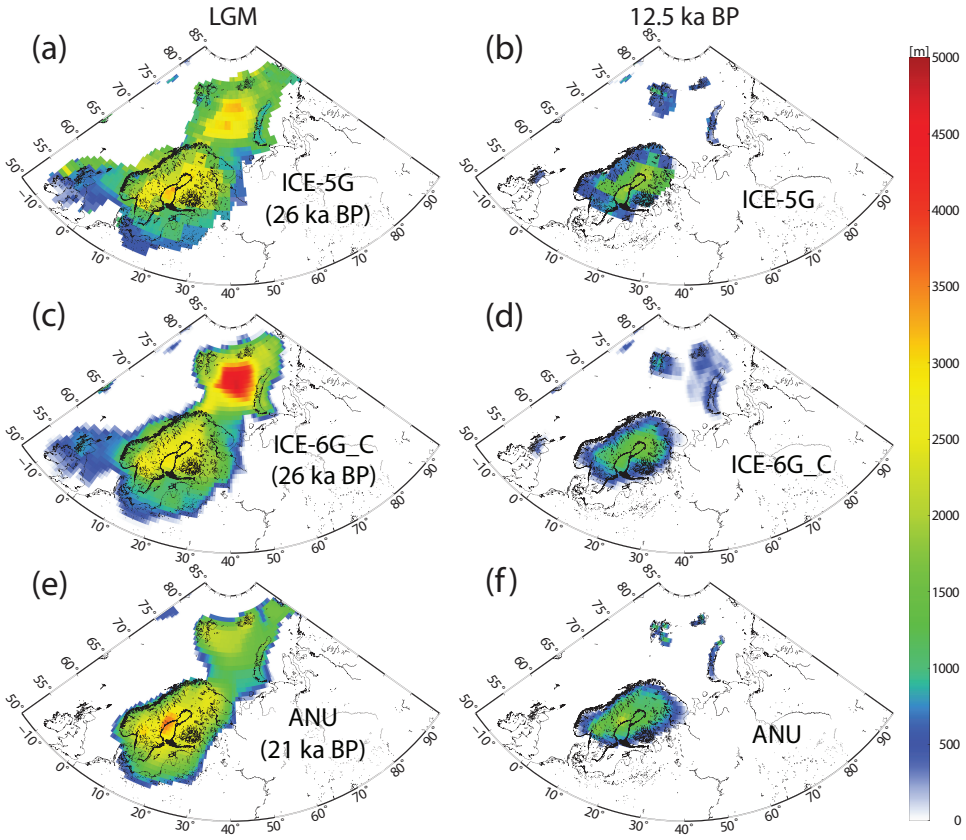

Figure 2: Ice extent and thickness (in metres, warm colours indicating thicker ice) from the ice load scenarios used in this study, at two different time steps: (left) LGM (which occurred at different times depending on the ice load scenario; age indicated in brackets on the plots and in the text) and (right) 12.5 ka BP. (a) and (b) are taken from the ICE-5G scenario, (c) and (d) from the ICE-6G_C scenario, and (e) and (f) from the ANU scenario.

ferent times for each of the scenarios; at ∼26 ka BP for both the ICE-5G and ICE-6G_C scenarios, at ∼24 ka BP for the S04 scenario, at ∼21 ka BP for the ANU scenario, and at ∼19 ka BP for the N05 and UiT scenarios. Finally, full deglaciation of the Barents Sea also takes place at slightly different times for each of the scenarios, the earliest being predicted by the N05 scenario at ∼14 ka BP and the latest by the UiT and ANU scenarios at ∼11.5 ka BP.

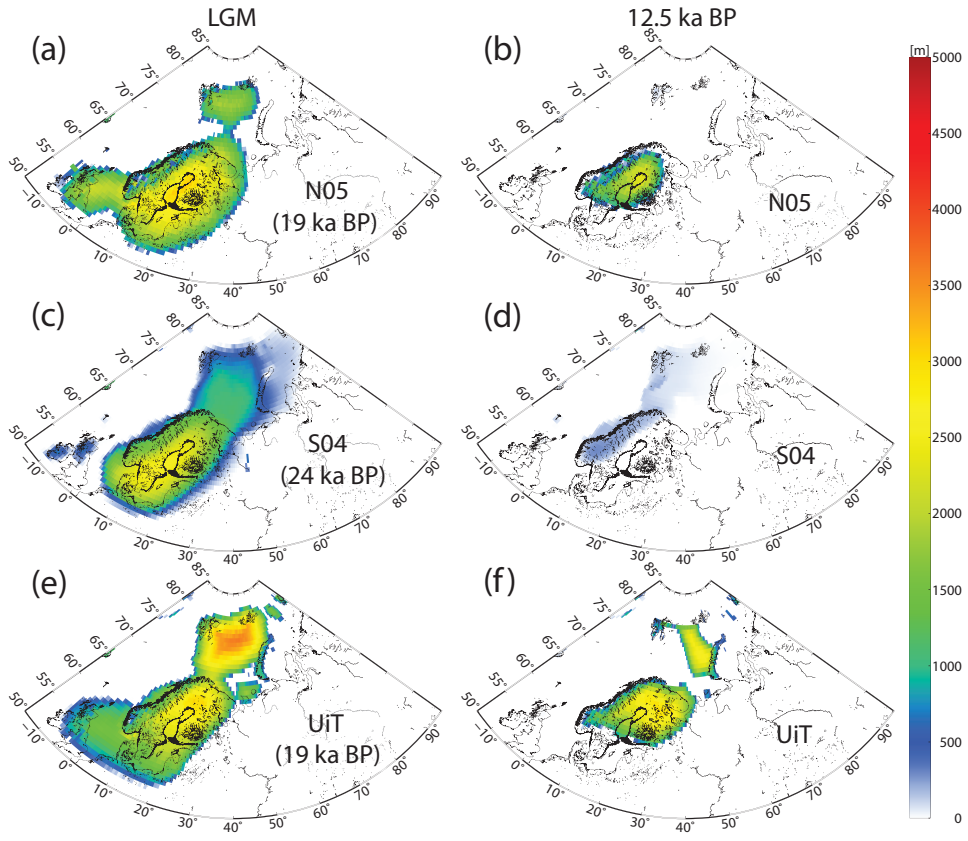

Figure 3: Same as Fig. 2 for the (a) and (b) N05 scenario, (c) and (d) S04 scenario, and (e) and (f) UiT scenario.

In order to solve the sea-level equation, we require a global ice load scenario. For each local scenario, we therefore used the ice thicknesses from ICE-5G in the far-field and replaced the ice thicknesses over Scandinavia and the Barents Sea with the predictions from the local scenarios. A nearest neighbour technique is used to combine the global and local models, whereby values from the closest point on the local grid are used to define ice thicknesses on the global grid. As well as covering different spatial extents, the scenarios cover different time spans, with the ICE-6G_C, S04 and UiT scenarios covering a shorter time (26–0 ka BP, 32–12 ka BP and 35–7.5 ka BP, respectively) than the ICE-5G, ANU and N05 scenarios (all spanning 122 ka BP to today). The ICE-6G_C scenario also starts with full glaciation over the Barents Sea and North America at 26 ka BP (contrary to the S04 and UiT scenarios which start with no ice in these regions and slowly build them up), therefore we implemented this scenario by linearly building up the load in these areas from 122 to 26 ka BP. All scenarios predict full deglaciation of the Barents Sea at latest by 11.5 ka BP. This is in line with field observations, which suggest that the main Barents Sea Ice Sheet had disappeared by the early Holocene (e.g. Landvik et al., 1998). Note, however, that it is likely that ice mass variations occurred on the ice caps located on the surrounding land of the Barents Sea during the Neoglacial and Little Ice Age (Svendsen and Mangerud, 1997), but that none of the scenarios we use include these Late Holocene ice caps nor account for their ice load changes (see discussion on this issue in Section 6). For the local models, recent ice mass variations in the far field (e.g. in Greenland) are accounted for by the ICE-5G load scenario. Finally, we investigated the effects of ice loading prior to 35 ka BP

by running an additional scenario. It includes the ice load from the ICE-5G model from 122 to 35 ka BP and the ice load from the UiT scenario from 35 ka BP onwards (see Section 6).

3 Sea-level and uplift observations

3.1 RSL data

Predicted relative sea-level changes output from our GIA modelling are compared with RSL data from localities around the Barents Sea (Fig. 1). Numerous studies of RSL have been published for this area, reflecting a long history of research from the 1960s (e.g. Blake, 1961; Hoppe et al., 1969) to the present day (e.g. Sessford et al., 2015). In order to obtain a consistent set of observations, particularly regarding the elevation uncertainties and reservoir corrections, we assembled all published data into our own database. This was based initially on the review paper by Forman et al. (2004) and all the references therein, to which we added more recent work (Romundset et al., 2011; Long et al., 2012; Sessford et al., 2015) and standardisation of the uncertainties.

For each location where observations on RSL have been made, we recorded the sampling elevation of each sample and the ^{14}C age along with its uncertainty (uncorrected for the reservoir effect). To be able to compare the RSL observations with the model predictions, the sampling elevations must

be expressed relative to mean tide level (MTL) with the age of the sample expressed in calibrated years before present (cal. a BP). To correct the elevation, we gathered information on the type of landform from which each sample was collected, based on the information given in each original publication, as well as the present-day elevation of storm beaches and the tidal range at each location (assumed constant through time). We attributed a consistent error for all samples whose elevations were measured using similar survey methods; assuming an uncertainty of ± 2 m if the sample elevation was obtained from maps or altimeters and ± 0.2 m for electronic distance measurements and levelling. This enabled us to correct and express each sample elevation relative to MTL, and assign a consistent estimate of the elevation uncertainty (using the propagation of errors). Moreover, we determined whether the sample was giving an estimate of the minimum, absolute or maximum position of mean sea level. Samples taken at the boundary between marine and lacustrine sediments in lakes give a precise estimate of the timing of isolation of the basin, and therefore provide a good estimate of MTL in the past. A few samples were however taken from slightly above or below the isolation boundary and therefore indicate a lower or upper limit of MTL at that time. The rest of the samples correspond to shells, driftwood and whalebones taken from raised storm beaches, i.e. features that formed during a major storm at some point in the past. Most of these samples can be related reasonably closely to the position of past MTL using the elevation of present-day storm beaches to correct for the contemporary sample offset from MTL. Samples that only provide a maximum or minimum constraint on past MTL are treated separately as one-sided bounds when comparing

the model predictions with the RSL observations (see Section 4). Finally, for the age of the samples, we assumed the same ΔR value of 100$\pm$39 yr for all sites around the Barents Sea, based on pre-bomb ages (Long et al., 2012), and obtained calibrated ages with CALIB v7.0.4 software, using the IntCal13 dataset for terrestrial samples and Marine13 for marine ones (Reimer et al., 2013).

The samples were split into 46 distinct geographically-constrained groups, each group showing the evolution of sea level through time at a particular location. For the scope of this study, we only used RSL data from locations where more than three samples were collected, and from locations which did not require significant assumptions (e.g. assuming the type of instrument used to measure the sample elevation if not mentioned in the original publication) to obtain an estimate of the uncertainties. This study considers RSL data from 46 locations, comprising 450 samples. We use the same location numbers as the ones presented in Forman et al. (2004), plus additional numbers for newer sites.

3.2 GPS data

In this study, we compared the predicted present-day rate of deformation in the Barents Sea and surrounding lands with vertical components of velocity estimates from GPS stations in Svalbard and northern Norway (Kierulf et al., 2014, Kierulf personal communication, 2014, Table 2). The stations in

northern Norway are continuous sites whereas stations in Svalbard and Bear Island are mostly campain sites. The GPS data were all processed using the GAMIT software and ITRF2008 reference frame, however, the uncertainties on the vertical uplift were calculated differently for the stations in Svalbard and TRO1 compared with the rest of the stations in Norway. For the former, the uncertainties correspond to the internal 1σ uncertainties obtained from the time series analysis, which have been suggested to be too optimistic (King et al., 2010). The latter were obtained using CATS (Williams, 2008), assuming a combination of both white and flicker noise (Kierulf et al., 2014), and are more reliable.

Stations NYAL, LYRS and SVES in Svalbard (Fig. 1) are all affected by present-day ice loss from nearby glaciers. As our ice load scenarios do not include such ice thickness changes, we used the estimate of 3.1 mm/a uplift caused by this ice loss from Omang and Kierulf (2011) to correct the vertical component observed at these stations. The uplift values indicated in Table 2 for these three stations have already been corrected for the present-day ice loss from nearby glaciers. No GPS station in Scandinavia is located near any of the few glaciers present in this region and therefore, present-day ice mass variations in Scandinavia are unlikely to have an impact on the observed velocities. Station HOPS, located on Hopen Island, is largely unstable and therefore has an unreliable vertical component (Kierulf personal communication, 2014).

Table 2: Present-day uplift rates and uncertainties from GPS stations in Svalbard and northern Norway.

Station name	Longitude	Latitude	Uplift [mm/a]	Uncertainty [mm/a]
NYAL	11.8651	78.9296	4.9	0.01[1]
BJOS	19.0014	74.5033	3.0	0.04[1]
HOPS	25.0137	76.5085	1.0	0.04[1]
LYRS	15.3973	78.2288	3.7	0.03[1]
SVES	16.7246	77.8991	1.6	0.05[1]
TRO1	18.9396	69.6627	3.6	0.02[1]
ANDO	16.0087	69.2784	1.3	0.40
TROM	18.9383	69.6627	2.7	0.29
VARS	31.0312	70.3364	2.8	0.32
HONS	25.9649	70.9771	1.7	0.60
ALTC	23.2962	69.9768	3.7	0.60
BALC	19.2265	69.2403	2.4	0.58
BJAC	16.5652	69.0003	2.3	0.45
FINC	17.9872	69.2312	3.4	0.59
KVAK	22.0570	69.7211	3.4	1.05
LOPC	22.3486	70.2394	3.6	0.63
OLDC	20.5344	69.6042	3.6	0.90
SKJC	20.9760	70.0345	2.6	0.81

[1] Underestimated one-sigma uncertainties obtained from the time series analysis.

4 Model-data comparison

For a single Earth model-ice load scenario, we compared the model predictions of sea level variation through time with the RSL data by calculating, for each sample at a particular location, a set of weighted residual sum of squares ($WRSS$) values such that

$$WRSS = \left(\frac{r_t}{\sigma_t}\right)^2 + \left(\frac{r_h}{\sigma_h}\right)^2 \quad (1)$$

where r_t is the residual in time, obtained as the difference between the age of the model prediction and the sample age, σ_t is the sample time uncertainty, r_h is the residual in elevation, obtained from the difference between the predicted elevation and the sample elevation, and σ_h is the sample elevation uncertainty. The $WRSS$ is calculated several times for each sample, comparing the sample age and elevation to all predicted values for a given model (i.e. along a modelled RSL curve), until the minimum $WRSS$ value (representing the misfit for that model-sample combination) is obtained. Only the minimum $WRSS$ value for each sample is retained and these are summed to get the $WRSS$ estimate for each location, $WRSS_j$. As mentioned in Section 3.1, the $WRSS$ is calculated in a different way for those RSL samples which only indicate a minimum or maximum position of the MTL. To reflect whether a particular model passes above or below the sample elevation, for a minimum or maximum constraint respectively, we consider only the model predictions with the same age as the sample. We then set the $WRSS$ to 1 if the model prediction is on the correct side of the sample elevation and to 3 otherwise, therefore penalising models that do not respect the condition

399 implied by the sample. These limiting $WRSS$ values (where relevant) are
400 added to all the minimum values of $WRSS$ for each sample to obtain the
401 $WRSS_j$.
402
403 We then summed all the $WRSS_j$ estimates obtained from Eq. 1 for all
404 the locations around the Barents Sea to obtain a global χ^2_g estimate

$$\chi^2_g = \sum_{j=1}^{M} \frac{WRSS_j}{N_j} \tag{2}$$

405 where N_j is the number of samples at each RSL location, and M the number
406 of locations. Eq. 2 is implemented such that we obtain one χ^2_g value per Earth
407 model-ice load scenario combination. For each ice load scenario, the Earth
408 model with the lowest χ^2_g value indicates the best-fit model. Uncertainties on
409 the best-fit Earth parameters are difficult to obtain due to our low-resolution
410 sampling of the parameter space. The minimum estimate most likely falls
411 between models that have been tested.
412

413 5 Results

414 Results from the comparison between the modelled predictions of sea-level
415 change through time and the RSL observations are given in Table 3 and Figs.
416 4–7. They are presented for each of the four main terrestrial areas bordering
417 the Barents Sea: Svalbard, Franz Josef Land, Novaya Zemlya and northern
418 Scandinavia. A few RSL curves, selected as being representative of the full

Table 3: Best-fit scenarios

Model	χ^2_g	Lithosphere thickness [km]	Upper mantle viscosity [$\times 10^{21}$ Pa s]	Lower mantle viscosity [$\times 10^{21}$ Pa s]
ICE-5G[1]	34.3	96	0.5	1
ICE-6G_C[2]	15.3	71	0.2	2
ANU	18.1	120	0.5	2
N05	109.7	71	0.5	2
S04	843.9	46	0.3	10
UiT	66.6	120	2	50

[1] The best-fit upper and lower mantle viscosities inferred for this scenario are slightly lower than the average values used by Peltier (2004) in his VM2 model.
[2] The best-fit lithosphere thickness, upper and lower mantle viscosities inferred for this scenario are slightly lower than the average values used by Argus et al. (2014) and Peltier et al. (2015) in their VM5a model.

array of RSL curves, are presented for each of these regions. The full set of RSL plots is presented as supplementary material in Figure S1 and details of the best-fit model for each scenario are given in Table S1.

Table 3 presents the best-fit earth model parameters for each ice model, as well as the corresponding value of χ^2_g. The ice load scenarios with the lowest χ^2_g are the ICE-6G_C, ANU, ICE-5G and UiT scenarios but the fact that χ^2_g is in general much higher than 1 indicates that none of the ice load scenarios are able to reproduce the RSL observations simultaneously at all sites around the Barents Sea. This is also confirmed by Figs. 4–7, which show observed and predicted RSL changes at a selection of locations in Svalbard (Fig. 4), Franz Josef Land (Fig. 5), Novaya Zemlya (Fig. 6) and northern Scandinavia (Fig. 7).

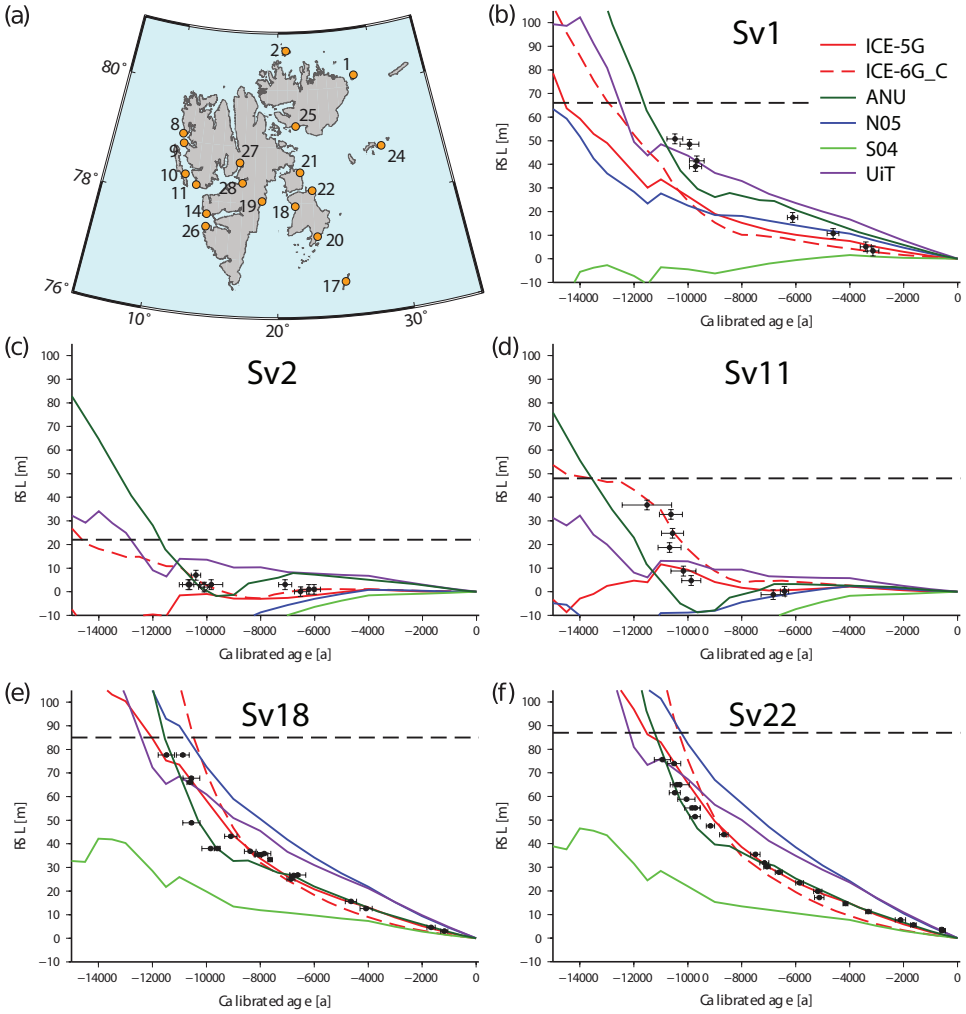

Figure 4: (a) Map showing the location of the RSL observations used in this study in Svalbard, and (b) to (f) comparison between the RSL data and model predictions for five locations (sites 1, 2, 11, 18 and 22, respectively). The black symbols and error bars show the observations and the coloured lines the model predictions according to the ICE-5G (in solid red line), ICE-6G_C (in dashed red line), ANU (in dark green), N05 (in blue), S04 (in light green) and UiT scenarios (in purple). The black dashed line gives the elevation of the marine limit. The diamond point at Sv2 represents a sample with a minimum constraint on the MTL.

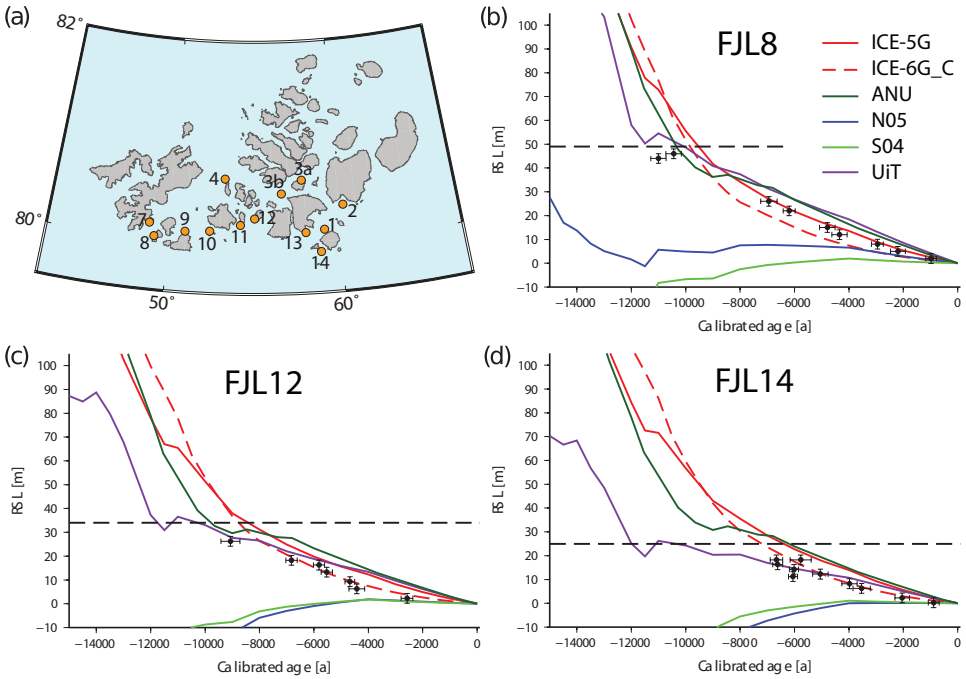

Figure 5: (a) Map showing the location of the RSL observations used in this study in Franz Josef Land, and (b) to (d) comparison between the RSL data and model predictions for three locations (sites 8, 12 and 14, respectively). The black symbols and error bars show the observations and the coloured lines the model predictions according to the ICE-5G (in solid red line), ICE-6G_C (in dashed red line), ANU (in dark green), N05 (in blue), S04 (in light green) and UiT scenarios (in purple). The black dashed line gives the elevation of the marine limit.

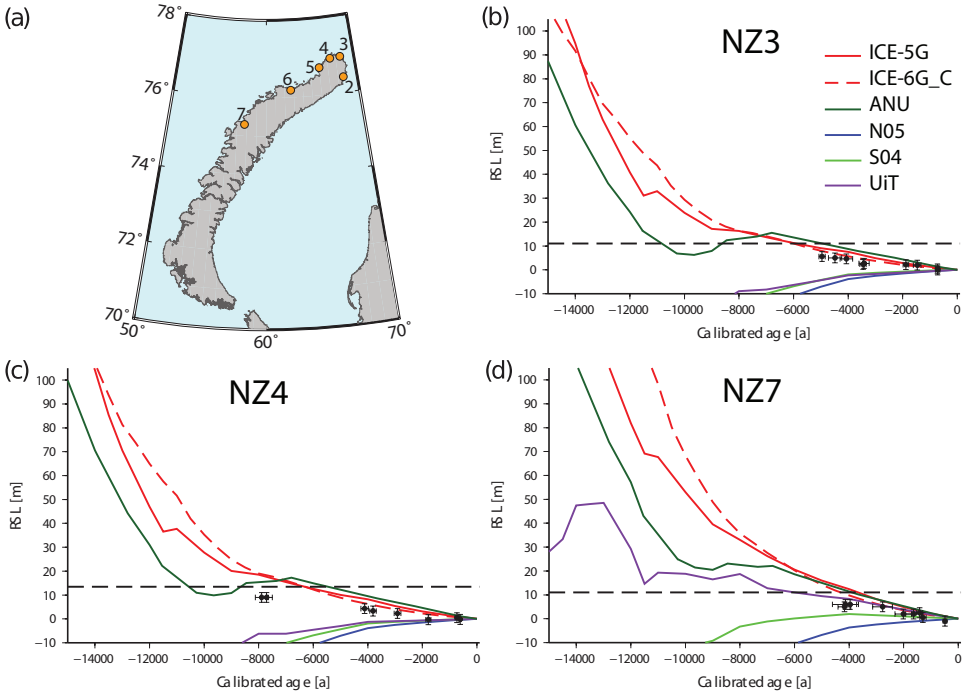

Figure 6: (a) Map showing the location of the RSL observations used in this study in Novaya Zemlya, and (b) to (d) comparison between the RSL data and model predictions for three locations (sites 3, 4 and 7, respectively). The black symbols and error bars show the observations and the coloured lines the model predictions according to the ICE-5G (in solid red line), ICE-6G_C (in dashed red line), ANU (in dark green), N05 (in blue), S04 (in light green) and UiT scenarios (in purple). The black dashed line gives the elevation of the marine limit.

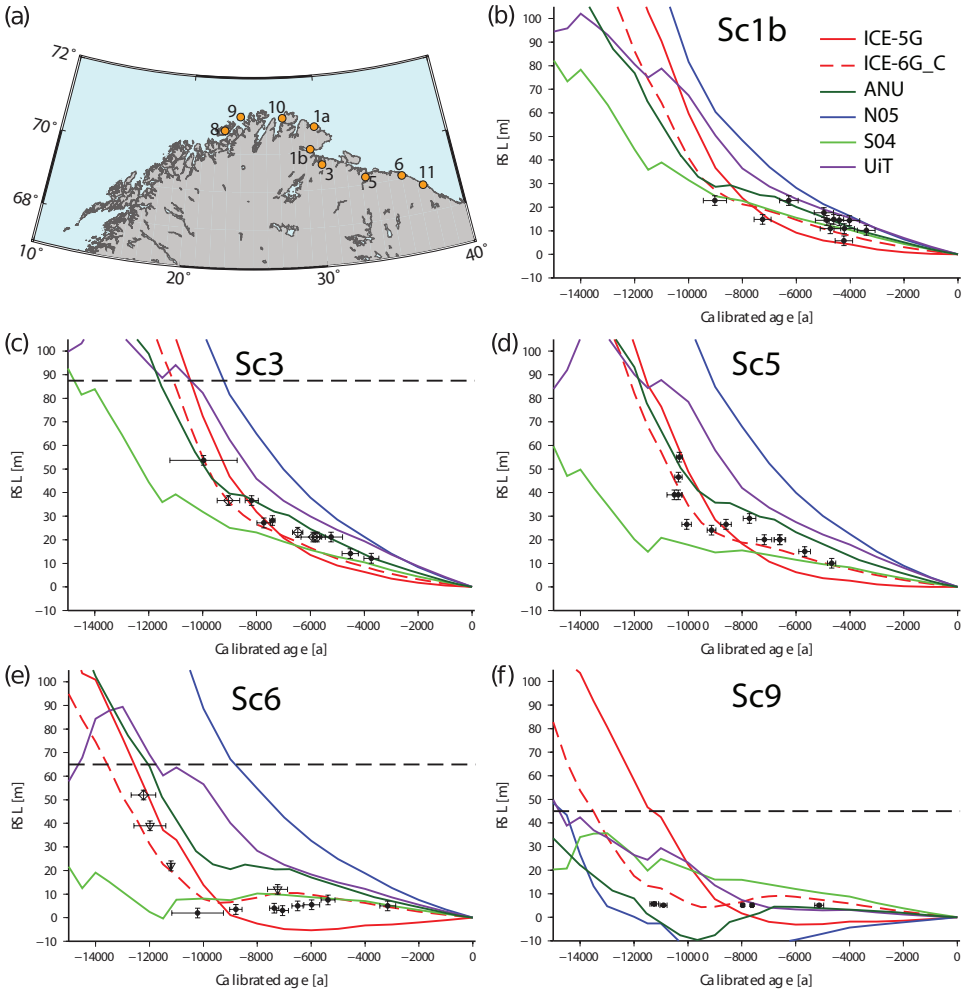

Figure 7: (a) Map showing the location of the RSL observations used in this study in northern Scandinavia, and (b) to (f) comparison between the RSL data and model predictions for five locations (sites 1b, 3, 5, 6, and 9, respectively). The black symbols and error bars show the observations and the coloured lines the model predictions according to the ICE-5G (in solid red line), ICE-6G_C (in dashed red line), ANU (in dark green), N05 (in blue), S04 (in light green) and UiT scenarios (in purple). The black dashed line gives the elevation of the marine limit, when observed. The diamond and triangle points at Sc3 and Sc6 represent samples with a minimum and maximum constraint on the MTL, respectively.

RSL observations in south-east Svalbard (locations 17 to 25, Fig. 4) are well fit by the predictions from the ICE-5G, ICE-6G_C, ANU, N05 and UiT scenarios, with a slight preference for the ANU model. The UiT and ANU scenarios give the best fit to the data in the north-east (location 1) and the ICE-6G_C model fits best along the west coast of Svalbard (locations 8 to 11, 14 and 26).

For Franz Josef Land (Fig. 5), predictions obtained with the ICE-5G, ICE-6G_C, ANU and UiT scenarios provide the best fit to the RSL observations, with a slight preference for the UiT scenario. The S04 and N05 scenarios have a very poor fit in this region as they predict a sea-level rise or stable sea-level during the early to mid-Holocene.

For the northern tip of Novaya Zemlya (Fig. 6), i.e. locations 2–5, the ICE-5G, ICE-6G_C and ANU scenarios fit the RSL observations equally well. For locations 6–7, further south on the west coast of the island, the UiT scenario yields a slightly better fit. In general, the predicted RSL curves are reasonably tightly clustered around the observations, however, the lack of data from prior to 8–5 ka BP makes it difficult to robustly infer a best-fit model for this region.

Finally, for northern Scandinavia (Fig. 7), the ICE-6G_C scenario best reproduces the RSL observations for most locations. At locations 1b and 11, the S04 scenario also gives a good fit and at location 1a, all scenarios apart from ICE-5G seem to match the observations.

These results show clearly that, overall, the S04 and N05 scenarios underestimate the RSL observations at the majority of sites around the Barents Sea and therefore require revision. This is to be perhaps expected as these ice load scenarios were developed at a time when fewer geological and geophysical data were available. Also, the N05 scenario was not optimised for the Barents Sea ice sheet in particular but for the Fennoscandian ice sheet. On the other hand, the ICE-5G, ICE-6G_C, ANU and UiT scenarios provide a much better fit to the data considering the wide spatial range of the observations. The better fit obtained with the ICE-5G, ICE-6G_C and ANU scenarios is not too surprising as these models are initially tuned with RSL data (even if the Earth structure we infer from our modelling is slightly different to the one used to build these scenarios). However, it is notable that the UiT scenario fits almost equally well to the RSL observations without being initially tuned to them.

As an independent validation of ice-loading scenario performance, Fig. 8 presents a fully independent comparison between GPS uplift measurements and vertical deformation predicted by the optimal Earth models using the ICE-5G, ICE-6G_C, ANU and the UiT scenarios. The comparison reveals that the best-fit model obtained with the ICE-5G (Fig. 8a) scenario is not able to match the GPS observations made in Svalbard, Bear Island and northern Scandinavia. Likewise for the UiT scenario (Fig. 8d) which also fails to constrain present-day recovery rates apart from at two GPS stations on the northeastern coast of Norway for which the fit is within uncertainties

(see Section 6). The ANU model agrees well with the GPS data throughout northern Norway, but does not match the data in the Barents Sea or on Svalbard. The present-day uplift predictions obtained for the best-fit Earth structure of ICE-6G_C (which has a thinner lithosphere and lower upper mantle viscosity than the other scenarios) is showing a slightly better agreement for GPS stations SVES, HOPS and BJOS, as well as some of the stations in northern Scandinavia. It is important to mention here that the uplift velocities we predict using the ICE-6G_C scenario are one order of magnitude lower than the velocities published by Peltier et al. (2015). This is partly due to the fact that the Earth structure we inferred for this scenario has a thinner lithosphere and lower upper mantle viscosity than the VM5a model used by Peltier et al. (2015).

6 Discussion

The six different ice-loading scenarios yield variable model performance on comparison to the database of RSL observations (Section 5), with the ICE-5G, ICE-6G_C, ANU and UiT scenarios giving the best fit overall. Although the ICE-5G and ICE-6G_C scenarios fit the data well, the ice thickness they provide for the Barents Sea appears overestimated, as observed by Root et al. (2015). If that is correct, we have to assume that the ice thickness provided by the UiT scenario is also overestimated, as it predicts a similar ice thickness over the Barents Sea as the ICE-5G and ICE-6G_C scenarios. The maximum Holocene model predictions from the ICE-5G, ICE-6G_C, ANU and

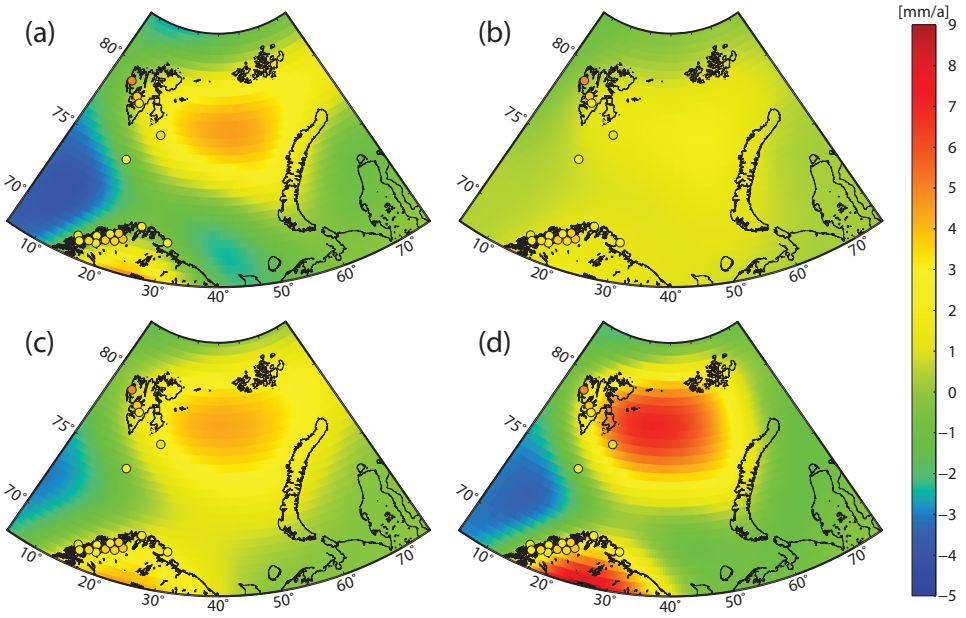

Figure 8: Predicted present-day uplift rates across the Barents Sea region for the (a) ICE-5G, (b) ICE-6G_C, (c) ANU and (d) UiT scenarios. In all cases, the relevant best-fit Earth model is used (see Table 3). GPS-observed uplift rates are also plotted (circles) using the same colour scale.

UiT scenarios typically lie well above the observed marine limit, which might not be an issue if the area was still covered by ice at that time. It is notable that the UiT scenario, not initially tuned to RSL data, fits the observations as well as the ICE-5G, ICE-6G_C and ANU scenarios. The ICE-5G, ICE-6G_C, ANU and UiT scenarios fit the RSL data in Franz Josef Land equally well even though their specific ice-loading history across the region contrasts markedly from one another. This is due to the fact that the best-fit Earth models for each of these scenarios are significantly different and manage to accommodate the disparities in ice load. In terms of empirical evidence however, the timing of ice mass variation given by the ICE-6G_C and ANU scenarios is probably more realistic. Regarding the S04 and N05 scenarios, although they do fit the data well in some areas, there are many areas where they fail to yield good RSL predictions. For the S04 scenario, we argue that the low maximum ice thickness and rapid deglaciation in the four regions studied is the main cause of the misfit between model and observations. This scenario also provides a lower bound estimate for the maximum thickness of the Barents Sea ice sheet. In the case of the N05 scenario, although the fit is relatively good for some locations in Svalbard and Scandinavia, it fails to reproduce the observations in the other regions, probably due to the fact that it has the lowest overall ice cover in the eastern and central Barents Sea, where the ice sheet only just merges with the Fennoscandian ice sheet.

An improved insight into local ice-loading performance can be obtained by optimising each model against RSL observations by region rather than globally. The resulting χ^2 values and best-fitting Earth model are presented

in Table 4. The χ^2 values are typically much lower, and the best fit is obtained by the ANU scenario for Svalbard and Franz Josef Land, ICE-5G and ICE-6G_C for Novaya Zemlya and N05 for Scandinavia. χ^2 values are in general lowest, sometimes < 1, for the Novaya Zemlya region. This is likely due to the fact that all the samples from this region are very young (less than 8 ka BP) compared with the samples from other regions. This makes it easier to fit the data as the model predictions are quite similar for all ice load scenarios, compared with the situation prior to 8 ka BP, where major differences are seen between the ice models. The χ^2 values < 1 can also be due to the fact that there is a limited spread of the samples in time or the fact that the uncertainties on the samples are overestimated for this region. Novaya Zemlya is a key location where RSL data from earlier in the Holocene would prove valuable in distinguishing between the ice load scenarios. On Svalbard, the regional χ^2 values are still relatively high. This is partly due to the fact that there are a lot more locations with RSL observations to be fit compared with the other regions. Some locations in Svalbard (locations 8 and 9) have samples scattered around different elevations at similar times, making them more difficult to fit.

Table 4: χ^2 and best-fitting Earth model obtained for a regional fit for each of our six ice load scenarios

Model	Svalbard				FJL				NZ				Scandinavia			
	χ^2	h^1	v_u^1	v_l^1	χ^2	h^1	v_u^1	v_l^1	χ^2	h^1	v_u^1	v_l^1	χ^2	h^1	v_u^1	v_l^1
ICE-5G	27.4	120	0.3	8	4.0	120	0.2	8	0.3	120	0.1	30	21.2	120	2	50
ICE-6G_C	12.8	96	0.3	3	3.5	120	0.3	1	0.3	120	0.1	8	10.5	71	0.2	2
ANU	11.0	96	0.3	3	1.9	120	0.3	5	0.4	120	0.2	8	10.4	71	2	1
N05	114.6	71	0.5	50	45.6	120	0.5	50	5.6	120	0.05	1	9.8	96	0.2	2
S04	1541.7	46	0.3	10	59.4	71	2	1	2.8	71	3	1	16.0	71	0.8	8
UiT	20.6	120	0.2	2	2.5	96	3	20	0.4	120	0.05	3	51.9	120	5	50

[1] The three numbers given here correspond to the lithosphere thickness h, in km, the upper mantle viscosity v_u ($\times 10^{21}$ Pa s), and the lower mantle viscosity v_l ($\times 10^{21}$ Pa s), respectively.

As described in Section 2.2, we also tested the influence of ice loading in the Barents Sea prior to 35 ka BP by running an additional scenario, in which we merge the ice load predicted by the ICE-5G scenario for the beginning of the glacial cycle with the ice load predicted by the UiT scenario for the later period. By recalculating the fit to the RSL observations using this scenario and plotting the best-fit models obtained against the RSL data, it is apparent that the RSL curves obtained with ice mass changes prior to 35 ka BP lie slightly higher than the ones with a shorter ice history (Fig. 9). Therefore, ice load changes prior to the LGM require further investigation, as in some locations they may affect the sea level recorded by the oldest data in our database. However, the further back in time we go, the more difficult it is to constrain the extent and volume of the ice sheet, in turn leading to greater uncertainty in the modelled RSL values. Also, as our RSL observations span at best the last 12–14 ka, it would be difficult to use them to constrain ice load changes occurring early in the glacial cycle; differences in glacial loading in the early stages of the glacial cycle will not significantly affect the model predictions over the time covered by our observations. Finally, the present-day rate of deformation appears insensitive to the specific ice configuration prior to 35 ka BP since a difference of only $\sim$1% is apparent between the uplift rates predicted by the model where just the UiT scenario is used and the model where it is merged with the ICE-5G scenario for the early time period.

The comparison between the predicted rate of present-day deformation and the GPS observations reveals a poor general performance (Fig. 8). For the stations in Svalbard, this is most likely due to the fact that none of

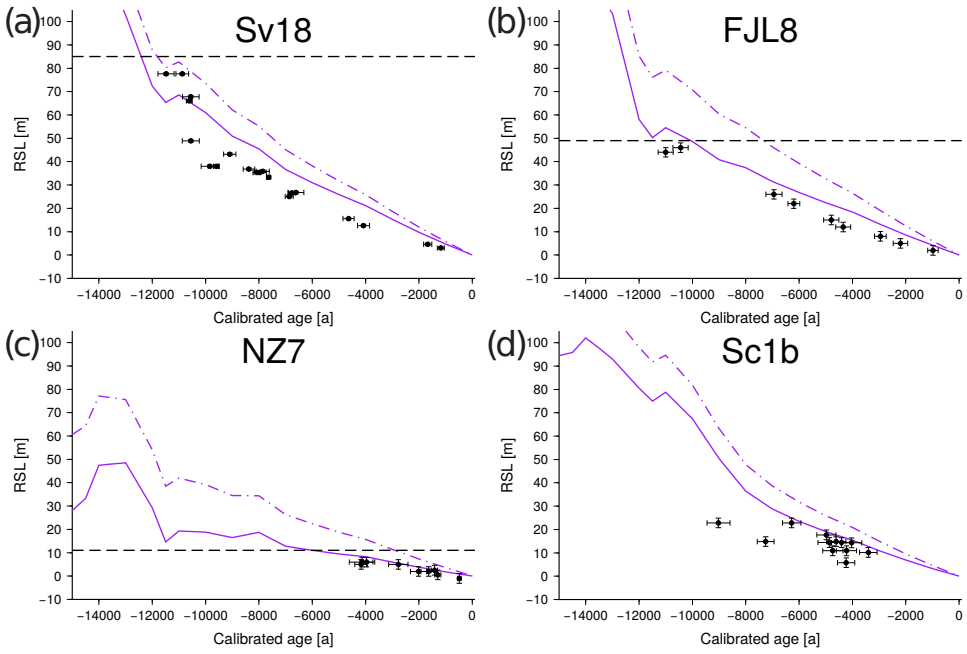

Figure 9: Comparison between the RSL data and model predictions for four locations around the Barents Sea showing the effects of pre-35 ka BP ice loading: (a) location 18 in Svalbard, (b) location 8 in Franz Josef Land, (c) location 7 in Novaya Zemlya and (d) location 1b in northern Scandinavia. The black points and error bars show the observations, and the purple lines are the model predictions according to the UiT scenario (continuous line) and the model merging the ICE-5G scenario for the early part of the last glacial cycle and the UiT scenario in the later part (dashed line).

the ice load scenarios used in this study account for ice load changes during the mid-to-late Holocene, in particular during the Little Ice Age (keeping in mind that the present-day ice melt has been corrected for at these stations). Melting of glaciers since the Little Ice Age can induce an uplift of the ground due to viscoelastic adjustment (e.g. Auriac et al., 2013), and this could at least partly account for the difference between the observed and predicted uplift rates. For the stations in northern Scandinavia, the misfit is most likely caused by the fact that the best Earth model inferred for the Barents Sea region is different from the one needed to obtain a good fit in Scandinavia. We argue that the stations with the best potential to constrain the ice load in the Barents Sea area are the ones least influenced by GIA in Scandinavia and the ones not influenced by present-day ice mass loss in Svalbard, leaving the two stations further east on the northern coast of Norway and station BJOS. The predicted uplift obtained with the best-fit model from the ICE-5G scenario significantly underestimates the GPS observations at these three stations. However, the predictions from the UiT and ANU scenarios are within the uncertainties for the two stations in northern Norway (Table 2), and only slightly underestimate the uplift at station BJOS. The ICE-6G_C scenario provides the best fit to these three stations but in general underestimates the deformation at the other GPS stations. Regarding the predicted uplift of these ice load scenarios, and noting that the Earth model is different for each of them, it seems likely that during deglaciation, the last ice mass was located in the northern part of the Barents Sea, where the maximum uplift is observed. This is also confirmed by some empirical data (Andreassen et al., 2014). It must be noted here that the GPS data, because of their sparse

and uneven spatial coverage, are not ideal to constrain the GIA modelling in the Barents Sea. Alternatively, Root et al. (2015) suggest that GRACE data may provide a more reliable method of determining the GIA signal across oceanic regions, where there are no data relating to past ice thickness or sea-level change.

Previous studies have used different techniques to investigate the rheological properties of the Earth in the Barents Sea region. Steffen and Kaufmann (2005) used paleoshorelines and GPS data to constrain their inverse modelling of GIA and infer the radial structure of the Earth in NW Europe and Scandinavia. They found that the observations could be best fit using a lithosphere thickness of $\sim$70 km and viscosities on the order of 10^{20} Pa s and 10^{22} Pa s for the upper and lower mantle in the Barents Sea region, respectively. Kaufmann and Wolf (1996) used RSL data to investigate the Earth model in the Barents Sea via theoretical modelling. Their results show that, for a fixed viscosity of 1×10^{21} Pa s for the lower mantle, the lithosphere thickness is likely to be higher than 110 km but poorly constrained, while they find that the viscosity of the upper mantle increases from west (10^{18}–10^{21} Pa s) to east (10^{20}–10^{21} Pa s) across the Barents Sea. Seismic observations have also been used to infer the structure of the Earth. For example, Klitzke et al. (2014) found that the depth of the lithosphere-asthenosphere boundary ranges from $\sim$70 to $\sim$150 km from west to east. Earth models preferred by our four best ice loading models (the ICE-5G, ICE-6G_C, ANU and UiT scenarios) are within the range of what has been found in previous studies. Keeping in mind that we only resolve well the upper mantle viscosity, we note

625 that the best-fitting Earth models obtained by region (Table 4) do not show
626 a lateral variation in the Earth model from west to east across the Barents
627 Sea. Uncertainties in the data and modelling as well as the low resolution
628 of our Earth parameter search probably would not allow us to resolve any
629 lateral variation if it were present. Finally, the distributions of the χ^2 val-
630 ues we obtain for each ice load scenario demonstrate that the RSL data we
631 use are not sensitive to the lithosphere thickness nor the lower mantle vis-
632 cosity. However, they prove better in constraining the upper mantle viscosity.
633
634 According to the results and discussion presented above, our study shows
635 that the RSL data from around the Barents Sea can be used to constrain
636 the ice model for the region as well as upper mantle viscosity. We show that
637 the current ice load scenarios available for the area are unable to fit con-
638 sistently all regions (Svalbard, Franz Josef Land, Novaya Zemlya or Scandi-
639 navia) through time. We argue that regions such as Novaya Zemlya or Franz
640 Josef Land, situated in the eastern part of the Barents Sea and presumably
641 located very close to the ice edge during the LGM, are important regions in
642 which to seek further RSL constraints because the ice history is still poorly
643 constrained in these regions. Since the ice load scenarios presented here do
644 not account for ice load changes during the Late Holocene, GPS uplift rates
645 observed in Svalbard cannot be fit with the model predictions. However, we
646 argue that the GPS station BJOS, as well as the stations located in northern
647 Norway, could be used to further constrain ice load reconstructions in the
648 Barents Sea region. Finally, our results seem to be in agreement with the
649 hypothesis that a single ice dome was centred on the Barents Sea during the

LGM. However, the ice thickness at the centre of the dome is particularly hard to constrain as no GPS or RSL observations can be obtained from close by.

7 Conclusions

Our study shows that the ice history of the Barents Sea can be investigated by comparing numerical modelling of GIA and past sea-level with near-field empirical RSL observations. We demonstrate that two of the ice load scenarios available for the area (the N05 and S04 scenarios) do not optimally capture the RSL observations but it should be noted that both scenarios are based on coupled climate-ice flow modelling, and are hence completely independent of RSL constraints unlike the ICE-5G, ICE-6G_C and ANU scenarios. Moreover, the NO5 scenario was not specifically intended or optimised for a Barents Sea ice sheet reconstruction and the SO4 experiments were conducted in an era when numerical ice sheet modelling and computing capacity was in its infancy and available paleo-climatic and marine-geological constraints were sparse. The ICE-5G, ICE-6G_C, ANU and UiT scenarios provide a relatively good fit to the RSL data, however, the ice thickness predicted by the ICE-5G, ICE-6G_C and UiT might be overestimated; this could be tested if older RSL data were available. The UiT scenario needs more work to be fully constrained, however, it shows great potential in providing a reliable ice load distribution for the Barents Sea during the last glaciation. Once fully independently constrained, this scenario will prove

very useful in investigating in greater detail the Earth model in this region, and potentially help resolve any lateral variations. The best-fit Earth models preferred by the ICE-5G, ICE-6G_C, ANU and UiT ice load scenarios fall within the bounds of the parameters inferred in previous studies using geophysical observations.

Aknowledgements

The authors would like to thank Martin Siegert, Jens-Ove Näslund, Kurt Lambeck and Anthony Purcell who kindly agreed to let us use their ice load scenarios, and Glenn Milne who developed the GIA model code used in this study. We would also like to thank Halfdan Kierulf who agreed to share his GPS data with us, and W. R. Peltier for making his ice load history models publicly available. The authors also thank two anonymous reviewers for their valuable comments and suggestions for the improvement of the manuscript. The research leading to these results has received funding from the People Programme (Marie Curie Actions) of the European Union's Seventh Framework Programme FP7/2007-2013/ under REA grant agreement n° 317217. The research forms part of the GLANAM (GLAciated North Atlantic Margins) Initial Training Network. PLW is supported by a NERC Independent Research Fellowship (NE/K009958/1). HP and AH acknowledge support from The Research Council of Norway through the PetroMaks project "Glaciations in the Barents Sea (GlaciBar)" (grant 200672) and its Centres of Excellence Scheme (grant 223259). All figures were made using

the Generic Mapping Tools, or GMT, package (Wessel and Smith, 1998).

References

Andreassen ,K., Laberg, J.S. and Vorren, T.O. Seafloor geomorphology of the SW Barents Sea and its glaci-dynamic implications. *Geomorphology*, 97:157–177, 2008. doi: 10.1016/j.geomorph.2007.02.050.

Andreassen, K., Winsborrow, M. C. M., Bjarnadóttir, L. R., and Rüther, D. C. Ice stream retreat dynamics inferred from an assemblage of landforms in the northern Barents Sea. *Quaternary Science Review*, 92:246–257, 2014. doi: 10.1016/j.quascirev.2013.09.015.

Argus, D. F., Peltier, W. R., Drummond, R. and Moore, A. W. The Antarctica component of postglacial rebound model ICE-6G_C (VM5a) based on GPS positioning, exposure age dating of ice thicknesses, and relative sea level histories. *Geophysical Journal International*, 198(1):537–563, 2014. doi: 10.1093/gji/ggu140.

Auriac, A., Spaans, K. H., Sigmundsson, F., Hooper, A., Schmidt, P., and Lund, B. Iceland rising: Solid Earth response to ice retreat inferred from satellite radar interferometry and visocelastic modeling. *Journal of Geophysical Research: Solid Earth*, 118:1331–1344, 2013. doi: 10.1002/jgrb.50082.

Bjarnadóttir, L. R., Winsborrow, M. C. M., and Andreassen, K. Deglaciation

of the central Barents Sea. *Quaternary Science Reviews*, 92:208–226, 2014. doi: 10.1016/j.quascirev.2013.09.012.

Blake, W. *Geology of the Arctic: proceedings of the first International Symposium on Arctic Geology, held in Calgary, Alberta, 1960, under the auspices of the Alberta Society of Petroleum Geologists*, chapter Radiocarbon dating of raised beaches in Nordaustlandet, Spitsbergen, pages 133–145. University of Toronto Press, Toronto, 1961.

Boulton, G. S. A model of Weichselian glacier variation in the North Atlantic region. *Boreas*, 8:373–395, 1979.

Brown, C., Meier, M. and Post, A. Calving Speed of Alaska Tidewater Glaciers, With Application to Columbia Glacier. *USGS Professional Paper 1258-C*, page 13, 1982.

Chambers, D. P., Wahr, J., Tamisiea, M. E., and Nerem, R. S. Ocean mass from GRACE and glacial isostatic adjustment. *Journal of Geophysical Research: Solid Earth*, 115:9, 2010. doi: 10.1029/2010JB007530.

Clark, P. U., Dyke, A. S., Shakun, J. D., Carlson, A. E., Clark, J., Wohlfarth, B. Mitrovica, J. X., Hostetler, S. W., and McCabe, A. M. The Last Glacial Maximum. *Science*, 325:710–714, 2009.

Dziewonski, A. M., and Anderson, D. L. Preliminary reference Earth model. *Physics of the Earth and Planetary Interiors*, 25:297–356, 1981.

Farrell, W. E., and Clark, J. A. On Postglacial Sea Level. *Geophys. J. R. astr. Soc.*, 46:647–667, 1976.

739 Forman, S. L., Lubinski, D. J., Ingólfsson, Ó., Zeeberg, J. J., Snyder,
740 J. A., Siegert, M. J., and Matishov, G. G. A review of postglacial
741 emergence on Svalbard, Franz Josef Land and Novaya Zemlya, north-
742 ern Eurasia. *Quaternary Science Reviews*, 23:1391–1434, 2004. doi:
743 10.1016/j.quascirev.2003.12.007.

744 Grosswald, M. G. and Hughes, T. J. The Russian component of an Arctic
745 Ice Sheet during the Last Glacial Maximum. *Quaternary Science Reviews*,
746 21:121–146, 2002.

747 Hoppe, G., Schytt, V., Häggblom, A., and Österholm, H. Studies of the
748 Glacial History of Hopen (Hopen Island), Svalbard. *Geografiska Annaler.*
749 *Series A, Physical Geography*, 51(4):185–192, 1969.

750 Hormes, A., Gjermundsen, E. F., and Rasmussen, T. L. From moun-
751 tain top to the deep sea – Deglaciation in 4D of the northwestern Bar-
752 ents Sea ice sheet. *Quaternary Science Reviews*, 75:78–99, 2013. doi:
753 10.1016/j.quascirev.2013.04.009.

754 Hubbard, A. High-Resolution Modeling of the Advance of the Younger Dryas
755 Ice Sheet and Its Climate in Scotland. *Quaternary Research*, 52:27–43,
756 1999.

757 Hubbard, A. The Verification and Significance of Three Approaches to Lon-
758 gitudinal Stresses in High–resolution Models of Glacier Flow. *Geografiska*
759 *Annaler*, 82:471–487, 2000.

760 Hubbard, A. The validation and sensitivity of a model of the Icelandic

ice sheet. *Quaternary Science Reviews*, 25(17–18):2297–2313, 2006. doi: 10.1016/j.quascirev.2006.04.005.

Hubbard, A. Sugden, D., Dugmore, A., Norddahl, H., and Pétursson, H. G. A modelling insight into the Icelandic Last Glacial Maximum ice sheet. *Quaternary Science Reviews*, 25:2283–2296, 2006. doi: 10.1016/j.quascirev.2006.04.001.

Hubbard, A., Bradwell, T., Golledge, N., Hall, A., Patton, H., Sugden, D., Cooper, R., and Stoker, M. Dynamic cycles, ice streams and their impact on the extent, chronology and deglaciation of the British-Irish ice sheet. *Quaternary Science Reviews*, 28:758–776, 2009. doi: 10.1016/j.quascirev.2008.12.026.

Hughes, T., Denton, G. H., and Grosswald, M. G. Was there a late-Würm Arctic Ice Sheet? *Nature*, 266:596–602, 1977.

Hughes, A. L. C., Gyllencreutz, R., Lohne, Ø. S., Mangerud, J., and Svendsen, J. I. The last Eurasian ice sheets – a chronological database and time-slice reconstruction, DATED-1 *Boreas*, 45:1–45, 2016. doi: 10.1111/bor.12142.

Ingólfsson, Ó., and Landvik, J. Y. The Svalbard-Barents Sea ice-sheet – Historical, current and future perspectives. *Quaternary Science Reviews*, 64:33–60, 2013. doi: 10.1016/j.quascirev.2012.11.034.

Kaufmann, G., and Wolf, D. Deglacial land emergence and lateral upper-mantle heterogeneity in the Svalbard Archipelago – II. Extended results

for high-resolution load models. *Geophysical Journal International*, 127: 125–140, 1996.

Kendall, R. A., Mitrovica, J. X., and Milne, G. A. On post-glacial sea lever – II. Numerical formulation and comparative results on spherically symmetric models. *Geophysical Journal International*, 161:679–706, 2005. doi: 10.1111/j.1365-246X.2005.02553.x.

Kierulf, H. P., Steffen, H., Simpson, M. J. R., Lidberg, M. Wu, P. and Wang, H. A GPS velocity field for Fennoscandia and a consistent comparison to glacial isostatic adjustment models. *Journal of Geophysical Research: Solid Earth*, 119:6613–6629, 2014. doi: 10.1002/2013JB010889.

King, M. A., Altamimi, Z., Boehm, J., Bos, M., Dach, R., Elosegui, P., Fund, F., Hernández-Pajares, M., Lavallee, D., Mendes Cerveira, P. J., Penna, N., Riva, R. E. M., Steigenberger, P., van Dam, T., Vittuari, L., Williams, S., and Willis, P. Improved Constraints on Models of Glacial Isostatic Adjustment: A Review of the Contribution of Ground-Based Geodetic Observations. *Surveys in Geophysics*, 31(5):465–507, 2010. doi: 10.1007/s10712-010-9100-4.

Klitzke, P., Faleide, J. I., Scheck-Wenderoth, M., and Sippel, J. A lithosphere-scale structural model of the Barents Sea and Kara Sea region. *Solid Earth Discussions*, 6:1579–1624, 2014. doi: 10.5194/sed-6-1579-2014.

Lambeck, K.. Constraints on the Late Weichselian ice sheet over the Barents Sea from observations of raised shorelines. *Quaternary Science Reviews*, 14:1–16, 1995.

Lambeck, K., Smither, C., and Johnston, P. Sea-level change, glacial rebound and mantle viscosity for northern Europe. *Geophysical Journal International*, 134:102–144, 1998.

Lambeck, K., Purcell, A., Funder, S., Kjær, H., Larsten, E., and Möller, P. Constraints on the Late Saalian to early Middle Weichselian ice sheet of Eurasia from field data and rebound modelling. *Boreas*, 35:539–575, 2006. doi: 10.1080/03009480600781875.

Lambeck, K., Purcell, A., Zhao, J., and Svensson, N.-O. The Scandinavian Ice Sheet: from MIS 4 to the end of the Last Glacial Maximum. *Boreas*, 39:410–435, 2010. doi: 10.1111/j.1502-3885.2010.00140.x.

Lambeck, K., Rouby, H., Purcell, A., Sun, Y., and Sambridge, M. Sea level and global ice volumes from the Last Glacial Maximum to the Holocene. *PNAS - Proceedings of the National Academy of Sciences of the United States of America*, 111(43):15296–15303, 2014. doi: /10.1073/pnas.1411762111.

Landvik, J. Y., Bondevik, S., Elverhøi, A., Fjeldskaar, W., Mangerud, J., Salvigsen, O., Siegert, M. J., Svendsen, J.-I., and Vorren, T. O. The Last Glacial Maximum of Svalbard and the Barents Sea area: Ice sheet extent and configuration. *Quaternary Science Reviews*, 17:43–75, 1998.

Le Meur, E., and Huybrechts, P. A comparison of different ways of dealing with isostasy: examples from modelling the Antarctic ice sheel during the last glacial cycle. *Annals of Glaciology*, 23:309–317, 1996.

828 Long, A. J., Strzelecki, M. C., Lloyd, J. M., and Bryant, C. L. Dating High
829 Arctic Holocene relative sea level changes using juvenile articulated marine
830 shells in raised beaches. *Quaternary Science Reviews*, 48:61–66, 2012. doi:
831 http://dx.doi.org/10.1016/j.quascirev.2012.06.009.

832 Mangerud, J., Dokken, T., Hebbeln, D., Heggen, B., Ingólfsson, Ó., Landvik,
833 J. Y., Mejdahl, V., Svendsen, J. I., and Vorren, T. O. Fluctuations of the
834 Svalbard-Barents Sea ice sheet during the last 150 000 years. *Quaternary*
835 *Science Reviews*, 17:11–42, 1998.

836 Mangerud, J., Svendsen, J. I., and Astakhov, V. I. Age and extent of the
837 Barents and Kara ice sheets in Northern Russia. *Boreas*, 28:46–80, 1999.

838 Marshall, S. J., Björnsson, H., Flowers, G. E., and Clarke, G. K. C. Sim-
839 ulation of Vatnajkull ice cap dynamics. *Journal of Geophysical Research*,
840 110:25, 2005. doi: 10.1029/2004JF000262.

841 Mitrovica, J. X., and Milne, G. A. On post-glacial sea level: I. General
842 theory. *Geophysical Journal International*, 154:253–267, 2003.

843 Näslund, J.-O. Climate and climate-related issues for the safety assessment
844 SR-Can. Technical report, Svensk Kärnbränslehantering AB, Stockholm,
845 October 2006, October 2006.

846 Näslund, J.-O., Jansson, P., Fastook, J. L., Johnsom, J., and Andersson, L.
847 Detailed spatially distributed geothermal heat-flow data for modeling of
848 basal temperatures and meltwater production beneath the Fennoscandian
849 ice sheet. *Annals of Glaciology*, 40:95–101, 2005.

Oerlemans, J., and van der Veen, C. J. *Ice Sheets and Climate*. Reidel Publishing Company, Dordrecht, 216 pp, 1984.

Omang, O. C. D., and Kierulf, H. P. Past and present-day ice mass variation on Svalbard revealed by superconducting gravimeter and GPS measurements. *Geophysical Research Letters*, 38(22):5, nov 2011. doi: 10.1029/2011GL049266.

Ottesen, D., Dowdeswell, J. A., and Rise, L. Submarine landforms and the reconstruction of fast-flowing ice streams within a large Quaternary ice sheet: The 2500-km-long Norwegian-Svalbard margin (57°–80°N). *GSA Bulletin*, 117(7–8):1033–1050, 2005. doi: 10.1130/B25577.1;.

Patton, H., Andreassen, K., Bjarnadóttir, L. R., Dowdeswell, J. A., Winsborrow, M. C. M., Noormets, R., Polyak, L., Auriac, A., and Hubbard, A. Geophysical constraints on the dynamics and retreat of the Barents Sea ice sheet as a paleobenchmark for models of marine ice sheet deglaciation. *Reviews of Geophysics*, 53:48, 2015. doi: 10.1002/2015RG000495.

Peltier, W. R. Global Glacial Isostacy and the Surface of the Ice-Age Earth: The ICE-5G (VM2) Model and Grace. *Annual Reviews Earth and Planetary Sciences*, 32:111–149, 2004. doi: 10.1146/annurev.earth.32.082503.144359.

Peltier, W. R., Argus, D. F., and Drummond, R. Space geodesy constrains ice age terminal deglaciation: The global ICE-6G_C (VM5a) model. *Journal of Geophysical Research: Solid Earth*, 120:450–487, 2015. doi: 10.1002/2014JB011176.

Pollard, D., and DeConto, R. M. *Glacial Sedimentary Processes and Products. International Association of Sedimentologists Special Publication*, volume 39, chapter A coupled ice-sheet/ice-shelf/sediment model applied to a marine-margin flowline: forced and unforced variations, pages 37–52. Wiley-Blackwell, 2007.

Polyak, L., Forman, S. L., Herlihy, F. A., Ivanov, G., and Krinitsky, P. Late Weichselian deglacial history of the Svyataya (Saint) Anna Trough, northern Kara Sea, Arctic Russia. *Marine Geology*, 143:169–188, 1997.

Polyak, L., Niessen, F., Gataullin, V., and Gainanov, V. The eastern extent of the Barents-Kara ice sheet during the Last Glacial Maximum based on seismic-reflection data from the eastern Kara Sea. *Polar Research*, 27(2): 162–174, 2008. doi: 10.1111/j.1751-8369.2008.00061.x.

Reimer, P. J., Bard, E., Bayliss, A., Beck, J. W., Blackwell, P. G., Ramsey, C. B., Buck, C. E., Cheng, H., Edwards, R. L., Friedrich, M., Grootes, P. M., Guilderson, T. P., Haflidason, H., Hajdas, I., Hatté, C., Heaton, T. J., Hoffmann, D. L., Hogg, A. G., Hughen, K. A., Kaiser, K. F., Kromer, B., Manning, S. W., Niu, M., Reimer, R. W., Richards, D. A., Scott, E. M., Southon, J. R., Staff, R. A., Turney, C. S. M., and van der Plicht, J. IntCal13 and Marine13 radiocarbon age calibration curves 0–50,000 years Cal PB. *Radiocarbon*, 55:1869–1887, 2013.

Romundset, A., Bondevik, S., and Bennike,O. Postglacial uplift and relative sea level changes in Finnmark, northern Norway. *Quaternary Science Reviews*, 30:2398–2421, 2011. doi: 10.1016/j.quascirev.2011.06.007.

Root, B. C., van der Wal, W., Novák, P., Ebbing, J., and Vermeersen, L. L. A. Glacial isostatic adjustment in the static gravity field of Fennoscandia. *Journal of Geophysical Research: Solid Earth*, 120:503–518, 2015. doi: 10.1002/2014JB011508.

Sessford, E. G., Strzelecki, M. C., and Hormes, A. Reconstruction of Holocene patterns of change in a High Arctic coastal landscape, Southern Sassenfjorden, Svalbard. *Geomorphology*, 234:98–107, 2015. doi: doi:10.1016/j.geomorph.2014.12.046.

Siegert, M. J., Dowdeswell, J. A., and Melles, M. Late Weichselian Glaciation of the Russian High Arctic. *Quaternary Research*, 52:273–285, 1999.

Siegert M. J., and Dowdeswell, J. A. Numerical reconstructions of the Eurasian Ice Sheet and climate during the Late Weichselian. *Quaternary Science Reviews*, 23:1273–1283, 2004. doi: 10.1016/j.quascirev.2003.12.010.

Steffen, H., and Kaufmann, G. Glacial isostatic adjustment of Scandinavia and northwestern Europe and the radial viscosity structure of the Earth's mantle. *Geophysical Journal International*, 163:801–812, 2005. doi: 10.1111/j.1365-246X.2005.02740.x.

Svendsen, J. I., and Mangerud, J. Holocene glacial and climatic variations on Spitsbergen, Svalbard. *The Holocene*, 7:45–57, 1997.

Svendsen, J. I., Alexanderson, H., Astakhov, V. I., Demidov, I., Dowdeswell, J. A., Funder, S., Gataullin, V., Henriksen, M., Hjort, C., Houmark-Nielsen, M., Hubberten, H. W., Ingólfsson, Ó., Jakobsson, M., Kjær, H.,

Larsen, E., Lokrantz, H., Lunkka, J. P., Lysså, A., Mangerud, J., Matiouchkov, A., Murray, A., Möller, P., Niessen, F., Nikolskaya, O., Polyak, L., Saarnisto, M., Siegert, C., Siegert, M. J., Spielhagen, R. F., and Stein, R. Late Quaternary ice sheet history of northern Eurasia. *Quaternary Science Reviews*, 23:1229–1271, 2004. doi: 10.1016/j.quascirev.2003.12.008.

Waelbroeck, C., Labeyrie, L., Michel, E., Duplessy, J. C., McManus, J. F., Lambeck, K., Balbon, E., and Labracherie, M. Sea-level and deep water temperature changes derived from benthic foraminifera isotopic records. *Quaternary Science Reviews*, 21:295–305, 2002.

Wessel, P., and Smith, W. H. F. New, improved version of generic mapping tools released. *EOS, Trans. Am. Geophys. Un.*, 79(47):579, 1998.

Williams, S. D. P. CATS: GPS coordinate time series analysis software. *GPS Solutions*, 12:147–153, 2008. doi: 10.1007/s10291-007-0086-4.

Winsborrow, M. C. M., Andreasson, K., Corner, G. D., and Laberg, J. S. Deglaciation of a marine-based ice sheet: Late Weichselian palaeo-ice dynamics and retreat in the southern Barents Sea reconstructed from onshore and offshore glacial geomorphology. *Quaternary Science Reviews*, 29:424–442, 2010. doi: 10.1016/j.quascirev.2009.10.001.